

LETTER TO THE EDITOR

# CoRoT opens a new era in hot B subdwarf asteroseismology<sup>★,★★</sup>

## Detection of multiple $g$ -mode oscillations in KPD 0629–0016

S. Charpinet<sup>1</sup>, E. M. Green<sup>2</sup>, A. Baglin<sup>4</sup>, V. van Grootel<sup>1</sup>, G. Fontaine<sup>3</sup>, G. Vauclair<sup>1</sup>, S. Chaintreuil<sup>4</sup>, W. W. Weiss<sup>5</sup>,  
E. Michel<sup>4</sup>, M. Auvergne<sup>4</sup>, C. Catala<sup>4</sup>, R. Samadi<sup>4</sup>, and F. Baudin<sup>6</sup>

<sup>1</sup> Laboratoire d'Astrophysique de Toulouse-Tarbes, Université de Toulouse, CNRS, 14 Av. E. Belin, 31400 Toulouse, France  
e-mail: stephane.charpinet@ast.obs-mip.fr

<sup>2</sup> Steward Observatory, University of Arizona, 933 North Cherry Avenue, Tucson, AZ 85721, USA

<sup>3</sup> Département de Physique, Université de Montréal, CP 6128, Succursale Centre-Ville, Montréal, QC H3C 3J7, Canada

<sup>4</sup> LESIA, Observatoire de Paris, CNRS, Université Paris Diderot, 5 place Jules Janssen, 92190 Meudon, France

<sup>5</sup> Institute for Astronomy, University of Vienna, Türkenschanzstrasse 17, 1180 Vienna, Austria

<sup>6</sup> Institut d'Astrophysique Spatiale (IAS), bâtiment 121, 91405 Orsay Cedex, France

Received 14 April 2010 / Accepted 25 May 2010

### ABSTRACT

**Context.** The asteroseismic exploitation of long period,  $g$ -mode hot B subdwarf (sdB) pulsators has been a long sought objective undermined, thus far, by the difficulty of obtaining sufficiently precise and continuous time series data from the ground.

**Aims.** Fast photometry from space appears to be the only means of gathering the appropriate asteroseismic data for this type of star. We explore this possibility with the CoRoT (CONvection, ROTation, and planetary Transits) satellite.

**Methods.** We obtained  $\sim 24$  days of high quality, nearly continuous photometric data with CoRoT during a short run (SRa03) dedicated to the long period sdB pulsator KPD 0629–0016. We analysed the frequency (period) content of the CoRoT time series by combining Fourier analysis, nonlinear least squares fitting, and prewhitening techniques.

**Results.** Our study has led to the detection of a large number of  $g$ -mode pulsations in KPD 0629–0016, with 17 frequencies clearly identified in addition to 7 possible (although more uncertain) peaks emerging above the mean noise level (estimated at  $\sim 57$  ppm). This is more than is typically detected for sdB stars from the ground and, more importantly, the frequencies of all uncovered  $g$ -modes are, for the first time, reliably measured. This paves the way for a detailed asteroseismic analysis of this star. The oscillations are found in the 90–400  $\mu\text{Hz}$  frequency range with a dominant mode at 205.29  $\mu\text{Hz}$  ( $P = 1.353$  h) of amplitude 0.246% of the mean brightness, i.e., typical of mid-radial order  $g$ -mode pulsations.

**Conclusions.** These photometric observations of KPD 0629–0016 demonstrate that  $g$ -mode sdB pulsators have rich oscillation spectra that are accessible to current space-based facilities. CoRoT opens up a new era in asteroseismology of hot B subdwarf stars.

**Key words.** stars: oscillations – subdwarfs – stars: individual: KPD 0629–0016

## 1. Introduction

The occurrence of nonradial pulsations in some hot B subdwarf (sdB) stars provides an extraordinary tool for probing, by asteroseismic means, the inner structure and dynamics of stars that are representative of an intermediate stage of stellar evolution. SdB stars are associated with the so-called extreme horizontal branch (EHB) corresponding to low-mass ( $\sim 0.5 M_{\odot}$ ) objects burning helium in their core. They differ from classical horizontal branch stars mainly in terms of their residual H-rich envelope, which has been stripped down dramatically during the previous stage of evolution, leaving only a very thin layer less massive than  $0.02 M_{\odot}$ . For this reason, sdB stars are hot ( $T_{\text{eff}} \sim 22\,000\text{--}40\,000$  K) and compact ( $\log g \sim 5.2\text{--}6.2$ ), and never ascend the asymptotic giant branch before fading as white

dwarfs. It is unclear which mechanisms determine whether a star evolving through the red giant phase eventually loses (or not) all but a tiny fraction of its envelope. Close binary evolution through various channels is probably the main source of sdB stars (Han et al. 2002, 2003), but isolated main sequence progenitors passing through the red giant branch and experiencing, for some reason, enhanced mass loss cannot be totally excluded (D'Cruz et al. 1996).

Two classes of sdB pulsators provide the “basic material” for developing asteroseismology as a new investigation tool for this intermediate evolutionary stage. The sdBV<sub>r</sub> (or V361 Hya, or EC 14026; Kilkeny et al. 1997) stars oscillate rapidly with periods in the 100–600 s range, corresponding mostly to low-order, low-degree  $p$ -modes. These modes are driven by a classical  $\kappa$ -mechanism occurring in the zone of partial ionization of the iron-group elements (the Z-bump) and powered-up by radiative levitation (Charpinet et al. 1996, 1997). The sdBV<sub>s</sub> (or V1093 Her; Green et al. 2003) stars pulsate far more slowly with periods of  $\sim 1\text{--}2$  h, corresponding to mid-order gravity modes. The same mechanism drives these oscillations (Fontaine et al. 2003).

\* The CoRoT space mission, launched on December 27th 2006, has been developed and is operated by CNES, with the contribution of Austria, Belgium, Brazil, ESA, Germany, and Spain.

\*\* Appendix A is only available in electronic form at <http://www.aanda.org>

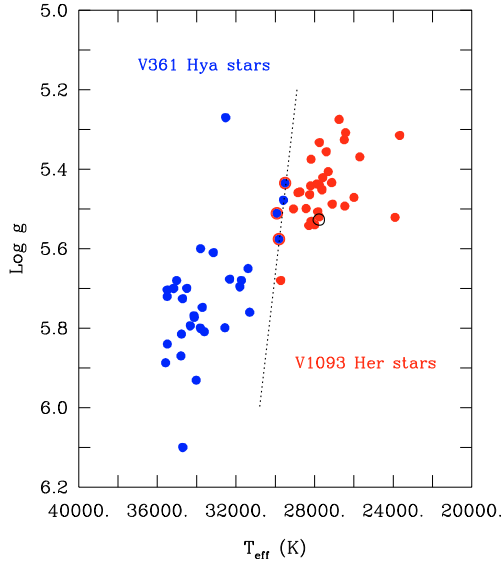


**Fig. 1.** Location of KPD 0629–0016 (black open circle) in the effective temperature-surface gravity plane in relation to the other known pulsating hot B subdwarf stars using a sample with reliable and homogeneous spectroscopic measurements. The short-period  $p$ -mode pulsators (V361 Hya stars) are shown in blue, while the long-period  $g$ -mode pulsators (V1093 Her stars) are shown in red. The three known hybrid stars showing simultaneously both  $p$ -mode and  $g$ -mode oscillations are also clearly indicated at the common boundary of both classes. KPD 0629–0016 belongs to the V1093 Her family.

A few stars belong to both classes and are called hybrid (or  $\text{sdB}_{\text{rs}}$ ) pulsators, showing both  $p$ - and  $g$ -modes (e.g., Schuh et al. 2006; see also the review by Charpinet et al. 2009).

Thus far, a dozen asteroseismic inferences have been successfully obtained from pulsating hot subdwarf stars (e.g., van Grootel et al. 2008a,b; Charpinet et al. 2008; Randall et al. 2009; Charpinet et al. 2009), but all were short period  $p$ -mode pulsators. The rapid oscillations associated with relatively large amplitudes ( $\sim 1\%$  of the mean brightness, but up to  $6\%$  in some cases) have indeed favoured these pulsators as preferred targets for seismic analysis based on data obtained from the ground. However, with the discovery of long period  $\text{sdB}$  pulsators, hope has grown that these could reveal the structure of the deepest regions in stars of this type, including the thermonuclear furnace. This is because  $g$ -modes in hot B subdwarf stars propagate toward the deep core, while  $p$ -modes remain confined to the outermost layers (Charpinet et al. 2000). However, despite valiant efforts from the ground (Randall et al. 2006a,b; Baran et al. 2009), it has been extremely difficult to differentiate the pulsation frequencies from the many aliases introduced by the lack of continuous coverage, particularly because of the much longer periods and the very low amplitudes (typically  $\sim 0.1\%$ ) involved. The asteroseismic study of  $g$ -mode  $\text{sdB}$  pulsators clearly requires accurate and continuous photometry in orbit.

The first attempt to observe a pulsating hot B subdwarf star from space was the MOST satellite monitoring for  $\sim 400$  h of the long period  $\text{sdB}$  star PG 0101+039 (Randall et al. 2005). While pulsations in this star were effectively detected based on these data, the very low amplitudes and the relative faintness of the target allowed the detection of only 3 frequencies, which are insufficient for a thorough asteroseismic study. This pioneering effort, however, left great hope that other stellar photometry satellites such as CoRoT (Baglin et al. 2006) and Kepler (Gilliland et al. 2010) would provide the needed breakthrough in this domain.

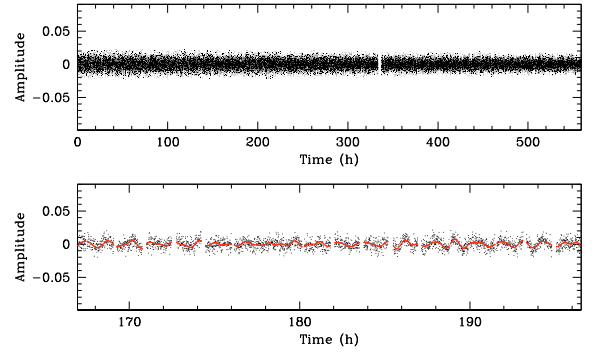


**Fig. 2.** CORoT light curve obtained for KPD 0629–0016 during SRa03 observations. The amplitude as a function of time is expressed in terms of the residual intensity relative to the mean brightness of the star. The red curve in the bottom panel shows the reconstructed signal based on the extracted frequencies, amplitudes, and phases given in Table 1.

KPD 0629–0016 is one of the few known  $\text{sdB}$  stars with a position in the sky compatible with CORoT field limitations. It was suspected and quickly confirmed by one of us (E.M.G.; followed by Koen & Green 2007) to be a  $g$ -mode pulsator on the basis of its atmospheric parameters ( $T_{\text{eff}} = 27\,780 \pm 270$  K and  $\log g = 5.527 \pm 0.041$ ), which are typical of  $\text{sdB}_{\text{V}}$  (V1093 Her) stars (see Fig. 1). It was therefore proposed in the framework of CORoT additional programs well before launch and subsequently selected as the primary target for the third short run in the Galactic anticentre direction (SRa03). Short runs are typically  $\sim 3$ – $4$  week observations scheduled right before or after flipping the satellite to keep the instrument away from direct sunlight. In this paper, we report the first asteroseismic observations of a hot B subdwarf pulsator with CORoT. In Sect. 2, we present the observations and frequency analysis of KPD 0629–0016. In Sect. 3, we compare our results with a representative model. We present our conclusions in Sect. 4.

## 2. Time series photometry and frequency content

The hot B subdwarf KPD 0629–0016 was observed by CoRoT over a time baseline of  $\sim 23.29$  days ( $\sim 558.96$  h) from March 5 to 29, 2010 (the scheduled SRa03 run). Because this star is relatively faint ( $V = 14.91$ ), it was positioned on a CCD dedicated to the planet finding program, which was designed to perform an accurate simultaneous photometric monitoring of thousands of stars in the 12–16 mag range. Every 32 s, except during a short interruption of  $\sim 3.55$  h at the end of day 13, a small image of KPD 0629–0016 was acquired. Basic reduction to remove known instrumental effects was performed by applying the standard reduction pipeline that produces exploitable light curves (see, e.g., Auvergne et al. 2009). The “white light” photometry obtained for KPD 0629–0016 reaches an effective duty cycle of  $\sim 80.5\%$ , leaving side lobes in the window function that are so small (less than  $8\%$ ) that they never interfere with the identification of real frequencies. Figure 2 shows the CORoT light curve for KPD 0629–0016. Low-amplitude multiperiodic oscillations with periodicities around  $\sim 1$ – $2$  h are clearly seen. This behaviour is typical of the  $\text{sdB}_{\text{V}}$  stars pulsating in mid-order  $g$ -modes on these timescales. We note that the complex interference pattern indicates that a significant number of modes are likely to be involved in the brightness modulation.

The Lomb-Scargle periodogram (LSP; Scargle 1982) of the light curve confirms the multiperiodic nature of the star brightness modulation (see Fig. 3). The region of interest, where

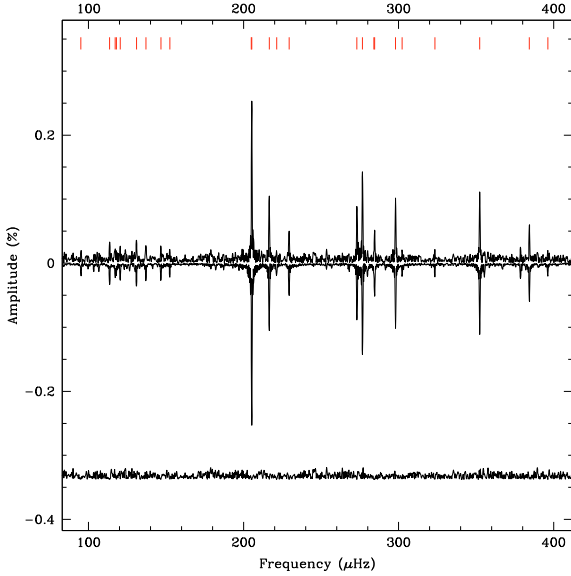


**Fig. 3.** Lomb-Scargle periodogram (LSP) in the 90–400  $\mu\text{Hz}$  frequency range where signal is found. The reconstructed LSP based on the 24 extracted harmonic oscillations given in Table 1 (indicated by red vertical segments) is shown upside down. The curve shifted downward is the LSP of the residual (i.e., noise) after subtracting all the frequencies in Table 1 from the observed light curve.

signal is clearly detected covers the range 90–400  $\mu\text{Hz}$ . Other frequency regions up to the Nyquist limit ( $\sim 15\,600\ \mu\text{Hz}$ ) are to be found consistent with noise. We applied the usual prewhitening and nonlinear least squares fitting techniques to extract the frequencies. We used a dedicated software, FELIX (Frequency Extraction for LIghtcurve eXploitation) developed by one of us (S.C.), that greatly eases and accelerates the application of this procedure, especially for space-based data. The procedure was performed with neither ambiguity nor difficulty, thanks to the very high quality of the CoRoT data.

We identified 17 frequencies,  $f_n$ , emerging above the usual  $4.0\sigma$  detection threshold. Table 1 provides the attributes (frequency, period, amplitude, phase, and signal-to-noise ratio) and their error estimates ( $\sigma_f$ ,  $\sigma_P$ ,  $\sigma_A$ , and  $\sigma_{\text{ph}}$ , respectively) resulting from the nonlinear least squares fit. We note that the phase is relative to the beginning of the run. We find that the noise level in this frequency range is extremely low, at  $\sim 0.0057\%$  (57 ppm). After prewhitening the 17 frequencies, a clear impression remained that power is still present in that particular frequency bandpass. This was particularly noticeable when comparing to regions where, clearly, no signal exists. While more uncertain (i.e., statistically less significant), we identified 7 additional peaks,  $u_n$ , listed in Table 1, with amplitudes between  $3.6$  and  $4.0\sigma$ , that could potentially be real.

The reconstructed light curve based on all the harmonic oscillations given in Table 1 is shown in Fig. 2 plotted (in red) over the observed light curve. In a similar way, Fig. 3 shows the Lomb-Scargle periodogram of the observed time series in the 90–400  $\mu\text{Hz}$  window and, plotted upside-down, its reconstruction based on all frequencies from Table 1. The LSP of the residual light curve after subtraction of all oscillations is also given, shifted downward. In both the time domain (Fig. 2) and frequency space (Fig. 3), the reconstruction based on the fitted modulations closely reproduces the observations.

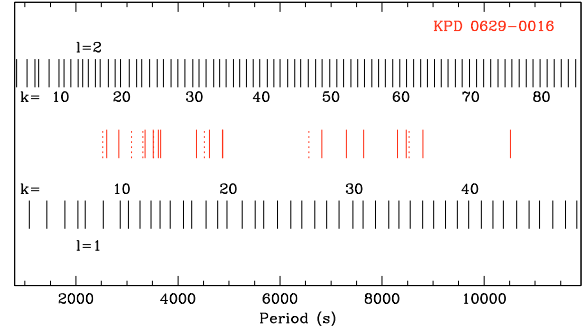


**Fig. 4.** Distribution of the 24 periods listed in Table 1 ( $f_1 - f_{17}$ : red segments;  $u_1 - u_7$ : dotted red segments) compared to the  $\ell = 1$  and  $\ell = 2$   $g$ -mode period distribution (black segments) in a representative sdB seismic model with surface parameters comparable to those measured for KPD 0629–0016. For each series of degree  $\ell$ , the radial order of the computed modes,  $k$ , is indicated.

### 3. Comparison with a representative model

Figure 4 shows the period distribution given in Table 1 compared to the low-degree ( $\ell = 1, 2$ ; the most likely observed modes for visibility reasons)  $g$ -mode pulsation spectrum of a model representative of KPD 0629–0016. We used our so-called third generation models (Brassard & Fontaine 2008, 2009), assuming a typical stellar mass  $M_* = 0.48 M_\odot$ , a fractional mass of the outer hydrogen rich envelope  $\log M_{\text{env}}/M_* = -2.5$ , a fractional mass of the convective core  $\log(M_{\text{core}}/M_*) = -0.25$ , and a core C+O mass fraction  $X(\text{C} + \text{O}) = 0.25$ . This structure leads to surface parameters  $\log g = 5.531$  and  $T_{\text{eff}} = 27\,319\ \text{K}$  that are close to the atmospheric values estimated from spectroscopy for KPD 0629–0016. We emphasize that it *does not* constitute a seismic solution of the observed period spectrum for this star. An accurate determination of the star structural parameters is beyond the scope of the present paper. This model simply provides a preliminary insight into the expected mode structure.

Figure 4 indicates that the observed modes in KPD 0629–0016 are relatively sparsely distributed compared to the computed spectrum. Groups of modes with possibly consecutive radial orders,  $k$ , are visible (in the 2500–4000 s range for instance), but between these groups some regions show no detectable pulsations even though the theoretical spectrum has modes in these area. The observed periods correspond to  $g$ -modes of radial order  $k$  between 9 and 44, if  $\ell = 1$ , and between 16 and 76, if  $\ell = 2$ . The mode density observed in the  $g$ -modes suggests that we are most likely observing a combination of  $\ell = 1$  and  $\ell = 2$  nonradial oscillations. Although the radial orders involved indicate that we are close to the asymptotic regime (except, maybe, for the lowest period modes), any attempt to isolate typical period spacings is problematic because sdB stars, in contrast to main sequence stars, are stratified objects with at least two zones of chemical transition in their interior producing significant trapping effects on  $g$ -modes. These combined effects perturb the simple uniform distribution predicted by the asymptotic pulsation theory as can be seen in Fig. 4. We, indeed, find no clear spacings between the periods given in Table 1. This is really not surprising because, in addition, only a fraction of the expected modes (according to the model) are effectively detected. The only reliable approach will be to match the pulsation spectrum in a detailed asteroseismic analysis.

**Table 1.** List of frequencies detected above  $4\times$  the local noise ( $f_n$ ) and above  $3.6\times$  the noise ( $u_n$ ).  $n$  is by order of decreasing amplitude.

Id.	Frequency ( $\mu\text{Hz}$ )	$\sigma_f$ ( $\mu\text{Hz}$ )	Period (s)	$\sigma_P$ (s)	Amplitude (%)	$\sigma_A$ (%)	Phase (s)	$\sigma_{\text{Ph}}$ (s)	$S/N$
$f_{17}$	95.0881	0.0654	10516.563	7.230	0.0243	0.0058	9196.211	512.076	4.2
$f_{12}$	113.5974	0.0461	8803.020	3.570	0.0342	0.0057	3097.336	306.998	5.9
$f_{16}$	117.9662	0.0650	8477.007	4.670	0.0243	0.0058	125.577	460.611	4.2
$f_{14}$	120.4154	0.0566	8304.588	3.904	0.0279	0.0058	5563.030	356.917	4.8
$f_{11}$	130.8794	0.0429	7640.621	2.505	0.0373	0.0058	3842.884	243.473	6.4
$f_{13}$	136.9661	0.0529	7301.076	2.818	0.0307	0.0059	6457.970	281.566	5.2
$f_{15}$	146.6156	0.0609	6820.557	2.835	0.0267	0.0059	1516.847	304.287	4.5
$f_{10}$	204.9958	0.0380	4878.150	0.904	0.0410	0.0057	2932.295	262.895	7.2
$f_1$	205.2887	0.0063	4871.190	0.150	0.2456	0.0057	3608.717	43.963	43.2
$f_4$	216.5288	0.0142	4618.324	0.303	0.1078	0.0056	2251.975	51.055	19.3
$f_8$	229.3277	0.0299	4360.573	0.569	0.0520	0.0057	1644.060	99.662	9.2
$f_6$	273.0739	0.0169	3662.012	0.227	0.0914	0.0056	2865.705	47.828	16.2
$f_2$	276.6529	0.0105	3614.638	0.137	0.1455	0.0056	1612.710	29.661	26.0
$f_9$	284.5848	0.0305	3513.892	0.377	0.0507	0.0056	3425.154	92.582	9.0
$f_5$	298.0091	0.0155	3355.602	0.174	0.1009	0.0057	2457.427	39.601	17.7
$f_3$	352.2916	0.0136	2838.557	0.110	0.1135	0.0056	2664.213	29.659	20.2
$f_7$	384.3322	0.0244	2601.915	0.165	0.0631	0.0056	1803.574	48.919	11.2
$u_1$	117.2195	0.0691	8531.006	5.027	0.0229	0.0058	7517.549	490.815	4.0
$u_4$	152.3785	0.0756	6562.604	3.258	0.0213	0.0059	3819.971	367.249	3.6
$u_2$	221.3004	0.0682	4518.744	1.392	0.0225	0.0056	1714.822	238.775	4.0
$u_5$	284.0690	0.0728	3520.271	0.903	0.0213	0.0056	866.705	113.756	3.8
$u_6$	302.2223	0.0733	3308.822	0.802	0.0211	0.0056	2066.142	186.802	3.7
$u_7$	323.3522	0.0693	3092.603	0.663	0.0217	0.0055	2569.895	168.049	4.0
$u_3$	396.1909	0.0768	2524.036	0.490	0.0201	0.0056	717.987	149.346	3.6

#### 4. Conclusion and prospects

The  $\sim 24$  day long CoRoT photometric observations of KPD 0629–006 presented in this paper allowed us to clearly uncover 17 (and possibly 24) frequencies in this star. Koen & Green (2007), observing from the ground, found only 6 frequencies, at most, with some large uncertainties caused by the low amplitudes and strong aliasing. Our results thus represent a vast improvement over what is achievable from the ground.

More generally, CoRoT demonstrates that contemporary high accuracy photometry obtained in space provides a decisive breakthrough in  $g$ -mode sdB pulsator characterisation. The key combined factors are the improved sensitivity, leading in the present case to a noise level of only 57 ppm in Fourier space, and the very high duty cycle that eliminates the aliasing problem. Even if large campaigns such as those of Randall et al. (2006a,b) and Baran et al. (2009) detected fairly large numbers of modes for some of the brightest known pulsators, the determination of their frequencies is unreliable for a large part, due to diurnal aliasing. This has catastrophic consequences for detailed asteroseismic studies because one daily alias ( $f \pm 11.57 \mu\text{Hz}$ ) mistakenly identified as the true frequency introduces an error between 3 and 12% for modes in the 400–100  $\mu\text{Hz}$  range. No reliable asteroseismic solution can be secured under these conditions (we recall that current asteroseismic solutions for sdB stars reach a typical accuracy of  $\sim 0.5\%$ ). With the present CoRoT observations of KPD 0629–0016, we have at last obtained a number of detected modes *with* secured frequencies, which, from our experience, is sufficient to provide a very solid basis for a detailed asteroseismic study similar to those conducted for the short period  $p$ -mode pulsators. CoRoT is undoubtedly opening a new era in hot B subdwarf asteroseismology that will permit the exploitation of  $g$ -modes as potential deep probes of the

internal structure of these stars. We have embarked in this venture by targeting KPD 0629–0016 and other stars of similar type that will benefit from space observations with the CoRoT and Kepler satellites.

#### References

- Auvergne, M., Bodin, P., Boissard, L., et al. 2009, A&A, 506, 411  
 Baglin, A., Auvergne, M., Barge, P., et al. 2006, ESA Spec. Publ., 1306, 33  
 Baran, A., Oreiro, R., Pigulski, A., et al. 2009, MNRAS, 392, 1092  
 Brassard, P., & Fontaine, G. 2008, ASPC, 392, 261  
 Brassard, P., & Fontaine, G. 2009, JPhCS, 172, 2016  
 Charpinet, S., Brassard, P., Fontaine, G., et al. 2009, in AIPCS 1170, ed. J. A. Guzik, & P. A. Bradley, 585  
 Charpinet, S., Fontaine, G., Brassard, P., & Dorman, B. 1996, ApJ, 471, L103  
 Charpinet, S., Fontaine, G., Brassard, P., et al. 1997, ApJ, 483, L123  
 Charpinet, S., Fontaine, G., Brassard, P., & Dorman, B. 2000, ApJS, 131, 223  
 Charpinet, S., van Grootel, V., Reese, D., et al. 2008, A&A, 489, 377  
 D’Cruz, N. L., Dorman, B., Rood, R. T., & O’Connell, R. W. 1996, ApJ, 466, 359  
 Fontaine, G., Brassard, P., Charpinet, S., et al. 2003, ApJ, 597, 518  
 Gilliland, R. L., Brown, T. M., Christensen-Dalsgaard, J., et al. 2010, PASP, 122, 131  
 Green, E. M., Fontaine, G., Reed, M. D., et al. 2003, ApJ, 583, L31  
 Han, Z., Podsiadlowski, P., Maxted, P. F. L., et al. 2002, MNRAS, 336, 449  
 Han, Z., Podsiadlowski, Ph., Maxted, P. F. L., & Marsh, T. R. 2003, MNRAS, 341, 669  
 Kilkeny, D., Koen, C., O’Donoghue, D., & Stobie, R. S. 1997, MNRAS, 285, 640  
 Koen, C., & Green, E. M. 2007, MNRAS, 377, 1605  
 Randall, S. K., Matthews, J. M., Fontaine, G., et al. 2005, ApJ, 633, 460  
 Randall, S. K., Fontaine, G., Green, E. M., et al. 2006a, ApJ, 643, 1198  
 Randall, S. K., Green, E. M., Fontaine, G., et al. 2006b, ApJ, 645, 1464  
 Randall, S. K., van Grootel, V., Fontaine, G., Charpinet, S., & Brassard, P. 2009, A&A, 507, 911  
 Scargle, J. D. 1982, ApJ, 263, 835  
 Schuh, S., Huber, J., Dreizler, S., et al. 2006, A&A, 445, L31  
 van Grootel, V., Charpinet, S., Fontaine, G., & Brassard, P. 2008a, A&A, 483, 875  
 van Grootel, V., Charpinet, S., Fontaine, G., et al. 2008b, A&A, 488, 685

## Appendix A: Details on the CoRoT time series analysis and frequency extraction

We provide additional technical details about the data acquisition, light curve analysis, and frequency extraction.

KPD 0629–0016 was monitored with a sampling time of 32 s. At each measurement, a small image (also called “imagette”) of the star was acquired, kept on board and transferred to the operation center. In the planet finding channel, the instrument is equipped with a small prism that produces a very low resolution spectrum on the CCD. When building photometric light curves, the pixel counts in the “imagette” are integrated into three separate time series corresponding to different colors (“red”, “green”, and “blue”). It is similar to broadband photometry, although with a limited wavelength coverage. Future exploitation of this color information needs to be investigated, but since our primary goal was to decrease as much as possible the noise level, we focused on the white light photometry produced by adding the counts of each color light curve at each time step.

For the analysis, we kept only data points that did not suffer from any reported perturbation (i.e., with flag set to zero). This excludes, most notably, measurements obtained during cyclic satellite transits across the South Atlantic Anomaly, which considerably degrades the accuracy and produces significant pollution in the data. The light curve was further de-trended for residual long term variations. Data points that significantly differ from the local standard deviation were removed by applying a running  $3\text{-}\sigma$  clipping filter. After all this filtering, the effective duty cycle dropped from  $\sim 99.3\%$  for the original data to  $\sim 80.5\%$ , but the periodograms are then vastly improved. The price to pay is the presence of side lobes in the window function, which, however, remain small and do not disturb the identification of true frequencies.

We applied the usual prewhitening technique to extract frequencies, one at a time: at each step of the procedure, the Lomb-Scargle periodogram (LSP) is computed, the highest peak in the frequency domain is selected and a cosine wave is fitted for frequency, amplitude, and phase to the time series data using a Levenberg-Marquardt nonlinear least squares algorithm. The fitted cosine wave is then subtracted from the data, resulting in the removal of the corresponding peak in the LSP (as well as its associated side lobes due to the window). The procedure is repeated until no more signal emerges over a given detection threshold above the noise (see below). Repeatedly, and at the end of the procedure, all cosine waves are fitted simultaneously using the nonlinear least squares routine.

The prewhitening sequence is illustrated in Fig. A.1. The top panel shows the LSP of the light curve in the  $90\text{--}400\ \mu\text{Hz}$  range. The 5 dominant (in amplitude) frequencies are indicated and the result of their prewhitening is then plotted in the panel below. The procedure continues with 4 additional frequencies removed, leading to the LSP represented in the panel further down. The frequency selection and removal proceeds until peaks no longer emerge above the detection threshold. Various thresholds are shown in Fig. A.1 corresponding to 4 times (green), 3.6 times (blue), and 3 times (red) the median noise level, respectively. This noise level is estimated locally by computing the median amplitude value within a running box of width  $\pm 1000$  frequency bins in the LSP. It is re-evaluated after each frequency prewhitening, such that, at the end of the procedure, the value obtained is representative of the true local noise contribution separated from the signal window pattern, even in crowded frequency regions containing several close peaks.

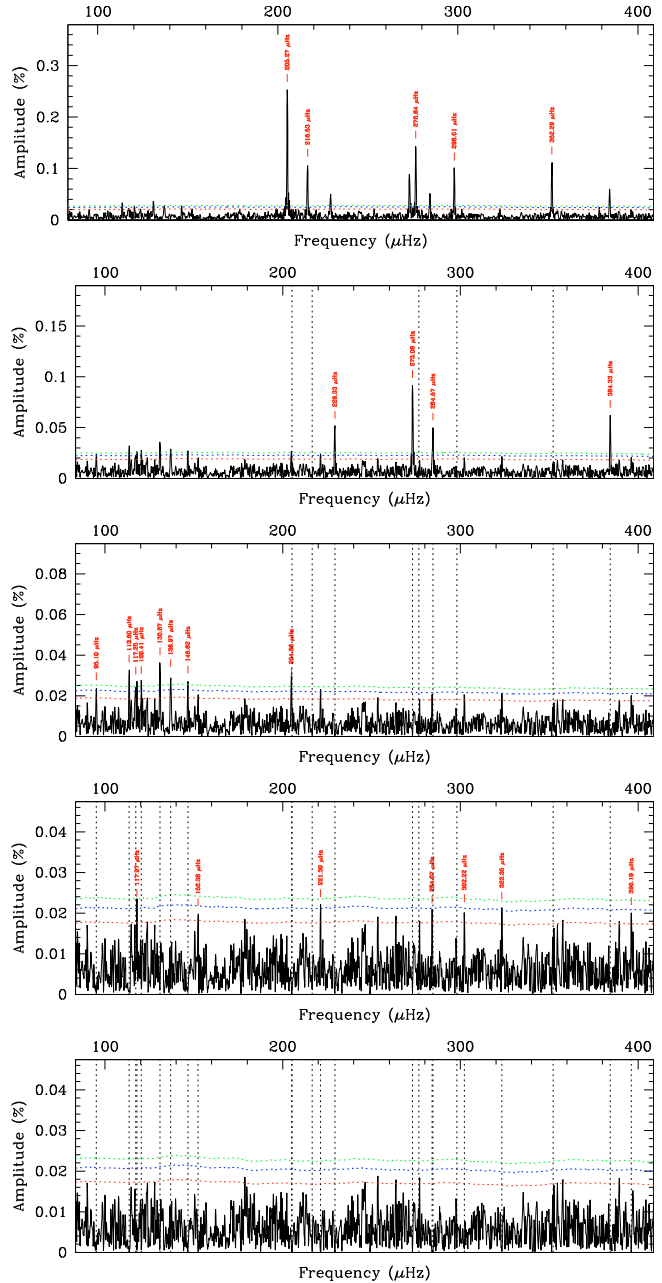


**Fig. A.1.** Lomb-Scargle periodograms (showing amplitude spectra in % of the mean brightness) and residuals after prewhitening of the identified frequencies in the CoRoT time series. The green (blue, red) dotted curves refer to a value equal to 4.0 (3.6, 3.0) times the local median noise level. Vertical dotted lines indicate the position of a peak previously removed.

It is usual to adopt the “ $4\text{-}\sigma$  criterion” as a safe limit for the detection of frequencies, which roughly corresponds to the 99.9% statistical significance level. All the peaks indicated in the 3 successive panels from the top in Fig. A.1 conform to this criterion, leading to the detection of 17 frequencies,  $f_n$ , given in Table 1. The 7 additional peaks,  $u_n$ , are identified in the fourth panel (from the top) in Fig. A.1. These have amplitudes between  $3.6$  and  $4.0\sigma$ .